The International Journal of Advanced Manufacturing Technology (2020) 110:1691–1700
https://doi.org/10.1007/s00170-020-05959-7

ORIGINAL ARTICLE

Geometric characteristic modeling for flexible contact of sanding wheel–polished complex surface

Wenbo Huai[1] · Xiaojun Lin[2] · Yaoyao Shi[2]

Received: 28 April 2020 / Accepted: 17 August 2020 / Published online: 27 August 2020

Abstract
The blade profile of a milled aeroengine blisk is a spatial free-form surface with significant curvature changes, which seriously restrict the quality uniformity of the polished surface. To investigate the geometric characteristics of the flexible contact of an elastic grinding tool–polished complex surface, a polishing process equipment integrating "CNC machine tool + flexible grinding head + elastic grinding tool" was used in this study. Through an analysis of the geometric theory, a mathematical model for the boundary between the sanding wheel and polished surface in the contact zone, a mathematical model for the compression amount in the contact zone, and a mathematical model for the removal depth were established to conduct simulation and polishing tests. The results show that both the compression amount of the sanding wheel and curvature radius on workpiece surface have remarkable effects on the boundary and removal depth in the contact zone; the feed speed, rotation speed, and particle size of the sanding wheel have no bearing on the boundary in the contact zone, but they can influence the removal depth markedly. The simulation results are basically consistent with the test results, proving that the established models are reliable and applicable to geometric characteristic prediction of the elastic grinding tool–polished complex surface.

Keywords Elastic grinding tool · Polishing · Complex surface · Flexible contact · Geometric characteristic · Modeling

1 Introduction

As a critical component of aeroengine, a blisk will have obvious scallop height and peak and trough after milling [1], which results in great surface roughness, and moreover, serious consequences like fatigue failure, deformation, or fracture under high-temperature and high-pressure environment [2]. Therefore, the surface roughness should be reduced using the polishing technology [3] to improve the fatigue resistance and surface friction properties of the blisk [4], improve the performance, and lengthen the service life of aeroengine. Hence, domestic (China) and foreign scholars have carried out a series of research work of guiding significance regarding polishing.

Kuo et al. [5] developed an Ace-Tone gaseous polishing system to polish an acrylonitrile-butadiene-styrene complex geometric structure part, which was prepared by a fused deposition model, using acetone vapor, thus reducing the surface roughness with favorable process stability. Xiao et al. [6] put forward a longitudinal micro-scratch measurement method for the rounded corner at blisk root based on the anti-fatigue machining principle, used point-to-point method to optimize the polishing path, conducted denoising and smoothing of grinding vectors, formed small uniform longitudinal micro-scratches, and improved the surface quality uniformity. For Ti-6Al-4V grinding, Liu et al. [7] implemented the preliminary optimization of grinding parameters through orthogonal test and signal-to-noise ratio (SNR) analysis, and obtained the optimal combination of grinding process parameters by taking material removal rate and specific grinding energy as the optimization objectives, and on this basis, they improved the grinding efficiency and surface quality. Following grey relational analysis of orthogonal test results, Zhang et al. [8] acquired the optimal combination of polishing process

✉ Wenbo Huai
huaiwb@xaut.edu.cn

[1] National Experimental Demonstration Teaching Center for Engineering Training, Xi'an University of Technology, Xi'an 710048, China

[2] School of Mechatronics, Northwestern Polytechnical University, Xi'an 710072, China

parameters for an abrasive belt and effectively reduced the roughness of the polished surface. In order to improve the quality of a laser-polished surface, Zhao [9] proposed the non-uniform rational B-splines (NURBS) to optimize the polishing path and improve the track precision. Gerhard et al. [10] elevated the damage threshold for laser polishing by optimizing the process conditions of glass preparation, and thus, the quality of laser-polished surface was remarkably improved. For blade polishing of aeroengine, Xiao et al. [11] studied the grinding cutting mechanism of a single abrasive particle, constructed a multi-particle parametric mathematical model, and proposed a grinding method for the micro-bionic zigzag surface of the abrasive belt, so as to improve the integrity of the polished surface. In order to improve the polishing quality of workpiece surface, Chen et al. [12] developed a magnetic and elastic grinding material to polish the inner surface of the workpiece under the attraction of ring magnet and the driving of turning pole, which reduced the polishing force and avoided the deep scratches on the workpiece surface. Liu et al. [13] conducted a numerical simulation in order to improve the polishing quality of abrasive particle flow in a micropore canal, acquired the optimal combination of the process parameters via an orthogonal test, and improved the polishing quality for abrasive particle flow in the micropore canal. Qi et al. [14] constructed a prediction model for the material removal depth through the abrasive belt polishing, and improved the model precision in full consideration of the influence of abrasive particle characteristics on the removal depth. Scholars represented by Shi et al. [2] developed the "CNC machine tool + flexible grinding head + elastic grinding tool (sanding wheel)" polishing process equipment for the aeroengine blisk with a complex structure, thin blade, and poor openness; proposed a polishing track programming method [15]; and optimized the process parameters by taking surface roughness and residual stress as the optimization objectives [2, 4]; however, as the blade curvature can change a lot, the compression amounts at different contact points between the sanding wheel and polished surface in the polishing process are different and present transient variation tendency, so the uniformity of the polishing quality is poor. Therefore, it is very essential to construct a reliable geometric model for flexible contact of the sanding wheel and a prediction model for the removal depth.

Based on the "CNC machine tool + flexible grinding head + elastic grinding tool (sanding wheel)" polishing process equipment, the complex surface polished by an elastic grinding tool—sanding wheel—was taken as the study object. Following an analysis of the geometric theory, a mathematical model for the boundary between the sanding wheel and polished surface in the contact zone, and a mathematical model for the removal depth were established. Their reliability was verified through the simulation and polishing tests.

2 Flexible contact model

The structure of the five-axis numerically controlled polishing lathe is shown in Fig. 1. This lathe includes 3 linear motion axes *X*, *Y*, and *Z*; 1 blisk rotation axis *C*; and 1 swing axis *A* of flexible grinding head; the key component of the equipment namely spindle head A of the flexible grinding tool is distributed with 3 micrometric displacement cylinders along the radial direction and installed with 1 micrometric displacement cylinder along the axial direction. In the polishing process, multiple displacement sensors distributed in radial direction and axial direction conduct real-time detection of pose change of the spindle tool. The acquired data signals are input into the industrial control system and calculated through the control algorithm in this system, control signals are output then so that air cylinders execute their actions and flexible spindle A does micrometric displacement action according to the geometric profile change of the blade, and the flexible spindle pose is adjusted in a real-time way so that the abrasive cloth wheel of the elastic grinding tool keeps fitting in with the geometric profile of the blade so as to realize adaptive flexible polishing [1, 4].

The sanding wheel under high-speed rotation will become very elastic due to the action of centrifugal force. Because of the normal polishing force at the contact point between the sanding wheel and blade surface, the sanding wheel undergoes elastic deformation and a micro-enveloping surface of "conformal micro-surface contact" is formed with the blade surface at the contact point [4], thus enlarging the area of the contact zone and improving the polishing efficiency. According to the Hertz contact theory, the micro-boundary formed between the sanding wheel and blade surface in the contact zone is approximated as an elliptical shape [14, 16].

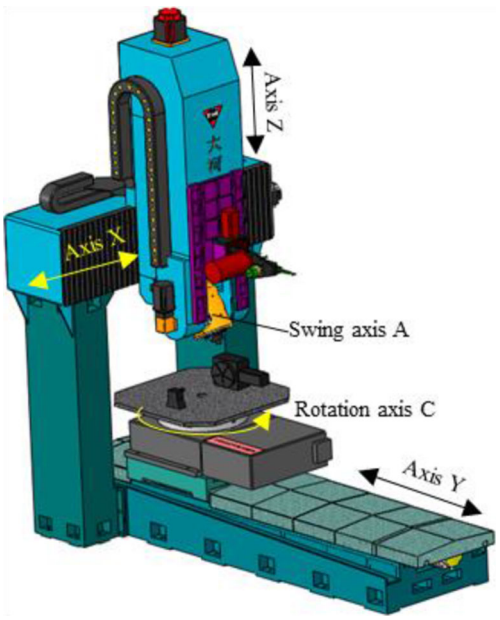

Fig. 1 Five-axis numerically controlled polishing lathe

2.1 Geometric model for contact zone

The sanding wheel can realize close conformal contact with the convex surface as shown in Fig. 2a, but its contact with the concave surface is not complete in the enveloping zone with "under-polishing" phenomenon as shown in Fig. 2b. To realize the complete contact with the concave surface, the sanding wheel is trimmed into a drum-type quadratic surface as shown in Fig. 2c.

A quadratic turning surface is taken as the polished surface in this study. The quadratic turning surface includes characteristics of both spherical surface and cylindrical surface, where R_1 is the maximum turning radius and profile radius of the surface, respectively. The drum-type sanding wheel has two characteristic radiuses r_1 and r_2, where r_1 is the maximum turning radius and r_2 is the surface radius of the sanding wheel. The geometric contact model between the drum-type sanding wheel and convex surface is shown in Fig. 3.

Figure 4 shows the K-directional view intercepted from the plane passing through the normal vector of the contact point and the axis of sanding wheel. In Fig. 4, the origin of the coordinate system $OXYZ$ is the center point of the contact zone, namely the position on the surface of the sanding wheel with the maximum compression amount δ_m. The coordinate axis X and coordinate axis Z are the directions of semi-major axis and semi-minor axis of the boundary in the contact zone, respectively. The coordinate axis Y is the direction where the workpiece center o_1 points at the center o_2 of the sanding wheel, that is, the normal vector direction of central contact point on the surface.

The workpiece center o_1 taken as the origin, central axis of the workpiece turning circle as axis x_1, and the direction same as the axis Y as axis y_1, the axis z_1 is determined according to the righthand rule and the coordinate system $o_1x_1y_1z_1$ is established; the arc center o_3 of the workpiece taken as the origin while the directions of other coordinate axes being identical with those in the coordinate system $o_1x_1y_1z_1$, the coordinate system $o_3x_3y_3z_3$ is constructed.

The center o_2 of the sanding wheel taken as the origin, the central axis of the sanding wheel turning circle as axis x_2, and the direction identical with the Y as axis y_2, the axis z_2 is determined according to the righthand rule, and the coordinate system $o_2x_2y_2z_2$ is constructed; The arc center o_4 of the sanding wheel taken as the origin while the directions of other coordinate axes being identical with those in the coordinate system $o_2x_2y_2z_2$, the coordinate system $o_4x_4y_4z_4$ is constructed.

a is the included angle between X and x_1 or x_3, β is the included angle between X and x_2 or x_4, and γ is the included angle between x_2 and x_1 or between x_4 and x_3. At the central point of the contact zone, the turning radius and arc radius of the workpiece are R_1 and R_2, respectively, and those of the sanding wheel are r_1 and r_2, respectively. ABC is the workpiece arc intercepted from the plane $o_3x_3y_3z_3$ and aOb is the sanding wheel arc intercepted from the plane $o_4x_4y_4z_4$. The maximum compression amount at the central point of the contact zone is δ_m, namely the distance between the origin O and point C.

To solve the compression amount at an arbitrary point in the contact zone, a point P is taken, and a straight line parallel to axis Y and intersecting with workpiece surface at point d and the sanding wheel surface at point e is drawn by passing through the point P. The turning section of the workpiece where the point d is located intersects with ABC at the point D, the turning section of the sanding wheel where the point e is located intersects with aOb at the point E, and the coordinates x and z of the point d and point e are identical with those of the point P (Fig. 4). The coordinates of these points in the coordinate system $OXYZ$ are marked as $P(x, y, z)$ $d(x_d, y_d, z_d)$, $e(x_e, y_e, z_e)$, $D(x_D, y_D, z_D)$, and $E(x_E, y_E, z_E)$, respectively, and they are expressed as $P(x_1, y_1, z_1)$, $d(x_{1d}, y_{1d}, z_{1d})$, $e(x_{1e}, y_{1e}, z_{1e})$, $D(x_{1D}, y_{1D}, z_{1D})$, and $E(x_{1E}, y_{1E}, z_{1E})$, respectively, in the coordinate system $o_1x_1y_1z_1$. The expression forms of these points in other coordinate systems can be acquired in a similar way.

2.2 Mathematical model for compression amount in contact zone

Here, the compression amount in the contact zone during the convex surface polishing is calculated. As shown in Fig. 4, y coordinate y_d of point d is firstly solved, and the coordinate transformation from the coordinate system $OXYZ$ into the coordinate system $o_1x_1y_1z_1$ is shown in Eq. (1).

$$\begin{cases} x_1 = x\cos\alpha - z\sin\alpha \\ y_1 = y + (R_1 - \delta_m) \\ z_1 = x\sin\alpha + z\cos\alpha \end{cases} \tag{1}$$

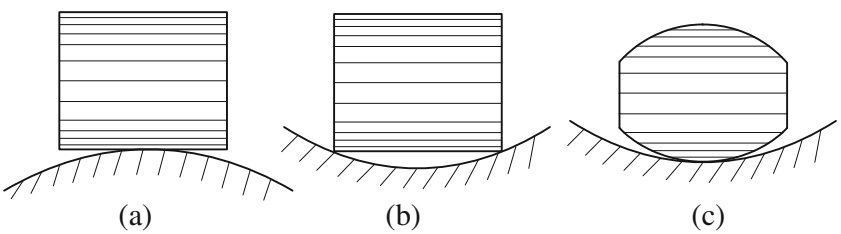

Fig. 2 Contact states between sanding wheel and surface

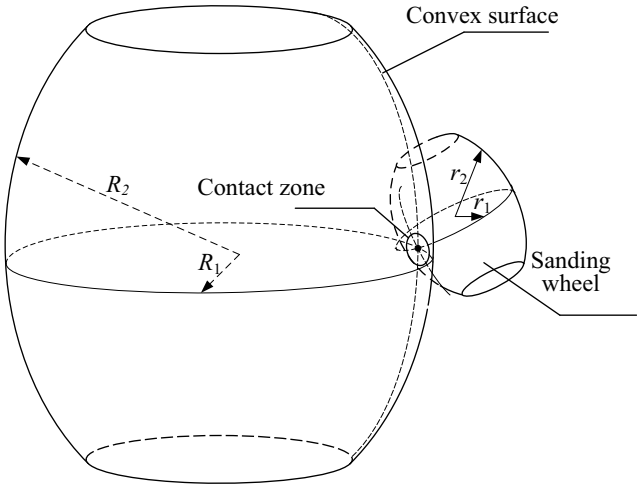

Fig. 3 Geometric contact model between sanding wheel and convex surface

The coordinate transformation from the coordinate system *OXYZ* into the coordinate system $o_3x_3y_3z_3$ is presented in Eq. (2).

$$\begin{cases} x_3 = x\cos\alpha - z\sin\alpha \\ y_3 = y + (R_2 - \delta_m) \\ z_3 = x\sin\alpha + z\cos\alpha \end{cases} \tag{2}$$

According to the geometrical relationship and relationship between the coordinate systems in Fig. 4, y coordinate of point d in the coordinate system *OXYZ* can be obtained as seen in Eq. (3).

$$y_d = \sqrt{\left[\sqrt{R_2{}^2 - (x_d\cos\alpha - z_d\sin\alpha)^2} + R_1 - R_2\right]^2 - (x_d\sin\alpha + z_d\cos\alpha)^2} - R_1 + \delta_m \tag{3}$$

Similarly, y coordinate y_e of point e in the coordinate system *OXYZ* can be solved according to $y_1 < r_1$ as seen in Eq. ((4).

$$y_e = -\sqrt{\left[\sqrt{r_2{}^2 - (z_e\sin\beta + x_e\cos\beta)^2} + r_1 - r_2\right]^2 - (z_e\cos\beta - x_e\sin\beta)^2} + r_1 \tag{4}$$

Therefore, the compression amount a_p at an random point $P(x, z)$s in the contact zone between the sanding wheel and workpiece can be known as seen in Eq. (5).

$$a_p = \int_{y_e}^{y_d} dy = y_d - y_e \tag{5}$$

Equations (3) and (4) are substituted into Eq. (5), and Eq. (6) can be obtained according to the geometrical relationship in Fig. 4.

$$a_p = \sqrt{\left[\sqrt{R_2{}^2 - (x\cos\alpha - z\sin\alpha)^2} + R_1 - R_2\right]^2 - (x\sin\alpha + z\cos\alpha)^2} + \sqrt{\left[\sqrt{r_2{}^2 - (z\sin\beta + x\cos\beta)^2} + r_1 - r_2\right]^2 - (z\cos\beta - x\sin\beta)^2} - R_1 - r_1 + \delta_m \tag{6}$$

Equation (7) can be acquired from Fig. 4.

$$\alpha = \gamma - \beta \tag{7}$$

The elastic contact area between the sanding wheel and the polishing surface is much smaller than the polished surface [17], and the tangential polishing force is so small that it can be neglected [18, 19]. Therefore, the deformation of sanding wheel can be considered as the Hertz's contact theory approximately. From the Hertz contact theory [14], it can be easily proved that β and γ satisfy Eq. (8).

$$\tan 2\beta = \frac{(1/R - 1/R')\sin 2\gamma}{1/r - 1/r' + (1/R - 1/R')\cos 2\gamma} \tag{8}$$

where $R = \max\{R_1, R_2\}$, $R' = \min\{R_1, R_2\}$, $r = \max\{r_1, r_2\}$, and $r' = \min\{r_1, r_2\}$, and α and β can be determined

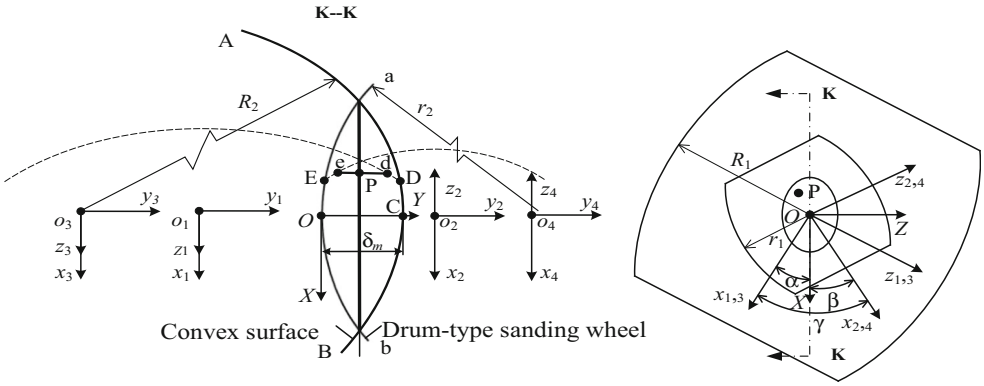

Fig. 4 Cross-sectional view of contact zone

through the included angle γ between the axis of the sanding wheel and workpiece axis.

To ensure that the sanding wheel agrees with the polished surface, the axis of the sanding wheel should be parallel to the tangential vector direction of the maximum principal curvature at the workpiece contact point in the polishing process [15] according to the polishing path programming technology, namely $\gamma = 0$. $\alpha = \beta = 0$ can be obtained according to Eqs. (7) and (8), and the compression amount at the time is seen in Eq. (9).

$$a_p = \sqrt{\left(\sqrt{{R_2}^2-x^2} + R_1-R_2\right)^2-z^2} + \sqrt{\left(\sqrt{{r_2}^2-x^2} + r_1-r_2\right)^2-z^2}-R_1-r_1 + \delta_m \tag{9}$$

The compression amount in the contact zone of the polished concave surface can be calculated in a similar way.

2.3 Mathematical model for boundary in contact zone

According to a related theory, the boundary between the sanding wheel and polished surface in the contact zone is an ellipse [14, 16] (Fig. 5). Therefore, the boundary can be obtained only if the semi-major axis and semi-minor axis of the ellipse are solved, and it is expressed by Eq. (10) in the coordinate system *XOZ*.

$$\frac{x^2}{{a_r}^2} + \frac{z^2}{{b_r}^2} = 1 \tag{10}$$

where a_r and b_r are the semi-major axis and semi-minor axis of the boundary in the elliptical contact zone, respectively.

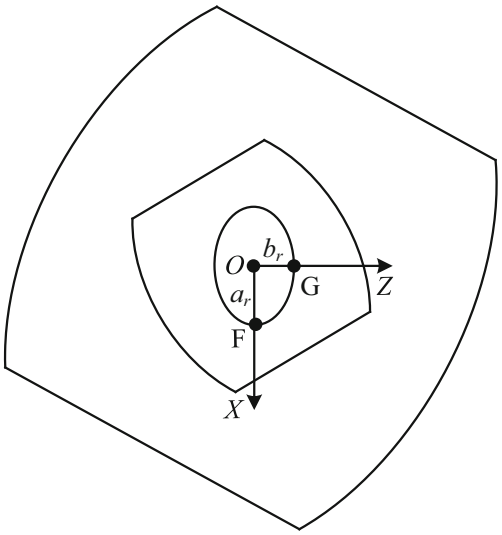

Fig. 5 Contact boundary between sanding wheel and workpiece surface

The convex surface is still taken as the study object. The coordinate x_F of vertex F on the elliptical semi-major axis is firstly calculated, and it can be known from Fig. 5 that point F in the coordinate system *OXYZ* satisfies Eq. (11).

$$\begin{cases} (y_F + R_1-\delta_m)^2 + (x_F \sin\alpha + z_F \cos\alpha)^2 = \left[\sqrt{{R_2}^2-(x_F \cos\alpha-z_F \sin\alpha)^2} + R_1-R_2\right]^2 \\ (y_F-r_1)^2 + (z_F \cos\beta-x_F \sin\beta)^2 = \left[\sqrt{{r_2}^2-(z_F \sin\beta + x_F \cos\beta)^2} + r_1-r_2\right]^2 \\ z_F = 0 \end{cases} \tag{11}$$

When the included angle between the sanding wheel and workpiece is $\gamma = 0$, Eq. (11) is expressed as Eq. (12).

$$\begin{cases} (y_F + R_1-\delta_m)^2 + {z_F}^2 = \left[\sqrt{{R_2}^2-{x_F}^2} + R_1-R_2\right]^2 \\ (y_F-r_1)^2 + {z_F}^2 = \left[\sqrt{{r_2}^2-{x_F}^2} + r_1-r_2\right]^2 \\ z_F = 0 \end{cases} \tag{12}$$

x_F can be solved as seen in Eq. (13).

$$x_F = \frac{\sqrt{\delta_m(2R_2-\delta_m)(2r_2-\delta_m)(2R_2 + 2r_2-\delta_m)}}{2(R_2 + r_2-\delta_m)} \tag{13}$$

Similarly, the coordinate z_G of vertex G on the semi-minor axis is calculated as seen in Eq. (14).

$$z_G = \frac{\sqrt{\delta_m(2R_1-\delta_m)(2r_1-\delta_m)(2R_1 + 2r_1-\delta_m)}}{2(R_1 + r_1-\delta_m)} \tag{14}$$

When the workpiece surface is a concave surface, the sizes of the semi-major axis and semi-minor axis of the boundary in the contact zone are seen in Eqs. (15) and (16).

$$x_F = \frac{\sqrt{\delta_m(2R_2 + \delta_m)(2r_2-\delta_m)(2R_2-2r_2 + \delta_m)}}{2(R_2-r_2 + \delta_m)} \tag{15}$$

$$z_G = \frac{\sqrt{\delta_m(2R_1 + \delta_m)(2r_1-\delta_m)(2R_1-2r_1 + \delta_m)}}{2(R_1-r_1 + \delta_m)} \tag{16}$$

2.4 Mathematical model for removal depth in contact zone

The local difference in the material removal depth exists due to different compression amounts in the elliptical contact zone. The direction of feed velocity is set as Z', and the coordinate system of the contact zone is *OXYZ*. In the meantime, the contact point taken as the origin, Z' as the feed direction and Y' as the normal direction of contact point, direction X' is determined according to the righthand rule, and the motion coordinate system $O'X'Y'Z'$ of the sanding wheel is constructed as shown in Fig. 6. By passing through one point $P'(x_0', z_0')$ in

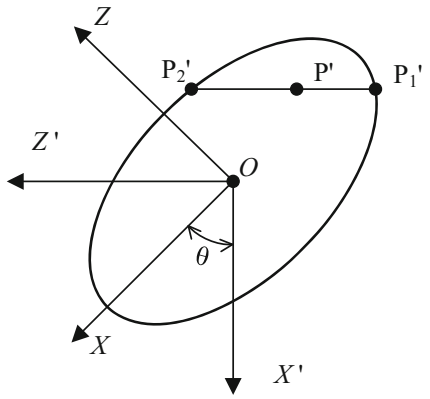

Fig. 6 Schematic diagram of integration path for polishing removal depth

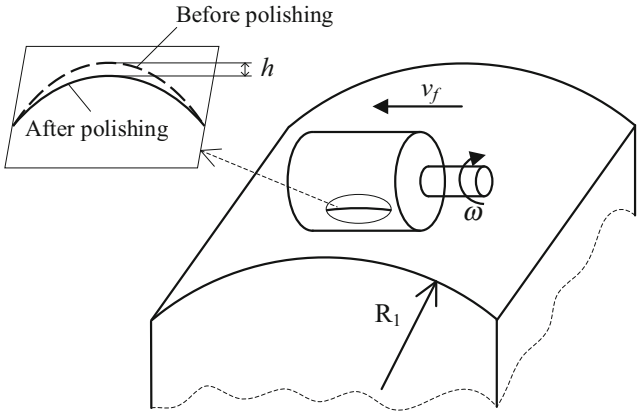

Fig. 7 Schematic diagram of simulation test

the contact zone, a straight line parallel to the feed direction Z' is drawn, which intersects with the boundary at points $P_1'\left(x_1', z_1'\right)$ and $P_2'\left(x_2', z_2'\right)$. As the contact zone is very small, it can be deemed that the polishing lengths passed by point P' and all points with x coordinate of x_0' are approximately equal and $z_2'-z_1'$.

The coordinate transformation from the coordinate system $X'OZ'$ into the coordinate system XOZ is seen in Eq. (17).

$$\begin{cases} x = x'\cos\theta + z'\sin\theta \\ z = -x'\sin\theta + z'\cos\theta \end{cases} \tag{17}$$

To simplify the expression form, related polynomials are simplified into the form shown in Eq. (18).

$$\begin{cases} l = a_r{}^2\sin^2\theta + b_r{}^2\cos^2\theta \\ m = \left(b_r{}^2 - a_r{}^2\right)\sin 2\theta \\ n = a_r{}^2\cos^2\theta + b_r{}^2\sin^2\theta \end{cases} \tag{18}$$

Equations (17) and (18) are substituted into Eq. (10), and then the coordinates of the boundary in the contact zone in the coordinate system $X'OZ'$ are obtained as seen in Eq. (19).

$$nz'^2 + mx'z' + lx'^2 - a_r{}^2 b_r{}^2 = 0 \tag{19}$$

z_1' and z_2' are two solutions of Eq. (19) as seen in Eq. (20).

$$\begin{cases} z_1' = \dfrac{-mx' - \sqrt{(mx')^2 - 4n\left(lx'^2 - a_r{}^2 b_r{}^2\right)}}{2n} \\ z_2' = \dfrac{-mx' + \sqrt{(mx')^2 - 4n\left(lx'^2 - a_r{}^2 b_r{}^2\right)}}{2n} \end{cases} \tag{20}$$

The compression amount in the coordinate system $X'OZ'$ is expressed as $a_p(x', z')$, and then the theoretical removal depth formed on the intersecting line $P_1'P_2'$ is seen in Eq. (21).

$$H(x_0') = \int_{z_1'}^{z_2'} K a_p(x_0', z')^{\beta_1} \omega^{\beta_2} v_f{}^{\beta_3} P^{\beta_4} dz' \tag{21}$$

where K is the proportionality coefficient related to the polishing material. a_p is the compression amount; ω is the spindle speed. v_f is the feed velocity, P is the abrasive particle size. β_1, β_2, β_3, and β_4 are undetermined coefficients.

The material removal depth and the coefficients in Eq. (21) are determined by abrasive grain size, workpiece hardness, polishing process parameters, and other factors, which increase the difficulty of modeling; therefore, using regression method makes calculation more convenient. The relevant References [2, 4, 18] show that the compression is the key parameter of the polishing force, and the polishing force is the key parameter of the material removal, so compression amount is the key parameter of the material removal. In this paper, compression amount modeling is accurate; other process parameters as a secondary factor of material removal have little effect on the accuracy of Eq. (21), and do not affect the prediction effect of the model.

3 Simulation and polishing tests

The surface removal depth h is defined as the value obtained by deducting the surface profile before polishing from the surface profile after polishing. In the simulation test and polishing test, the removal depth, passing through the contact point and being parallel to the direction of the polishing path, is measured as shown in Fig. 7.

The simulation test and polishing test conditions The workpiece material is TC4, the workpiece turning radius is R_1 = 18mm, $R_2 \to \infty$, namely the polished surface is a cylindrical surface; the turning radius of sanding wheel is r_1 = 6mm, $r_2 \to \infty$, and the width B is 12 mm, namely it is a cylindrical surface, the base material is fabric, and the abrasive particle is green silicon carbide (GC). The axis of the sanding wheel is

Table 1 Multiple linear regression coefficients

K	β_1	β_2	β_3	β_4
1.478	1.795	0.965	− 0.658	− 0.588

Table 2 Process parameters of polishing simulation test

δ_m (mm)	ω (r/min)	v_f (mm/min)	P	R_1 (mm)	r_1 (mm)
0.3/0.4	6500	200	400	18	6
0.4	5500/6500	200	400	18	6
0.4	6500	350/200	400	18	6
0.4	6500	200	600/400	18	6
0.4	6500	200	400	28/18	6

perpendicular to that of the cylindrical workpiece in the polishing process, the feed velocity v_f is parallel to the axis on the cylindrical surface of the workpiece, and then $\beta = 0^0$, $\gamma = \alpha = \theta = 90^0$ as shown in Fig. 7. The feeding direction along the sanding wheel axis, feeding speed v_f, and sanding wheel width B together determine the polishing time T, namely $T = B/v_f$.

According to the simulation and test conditions, the coefficients in Eq. (21) are acquired through the multiple nonlinear regressions of the orthogonal test results (Table 1).

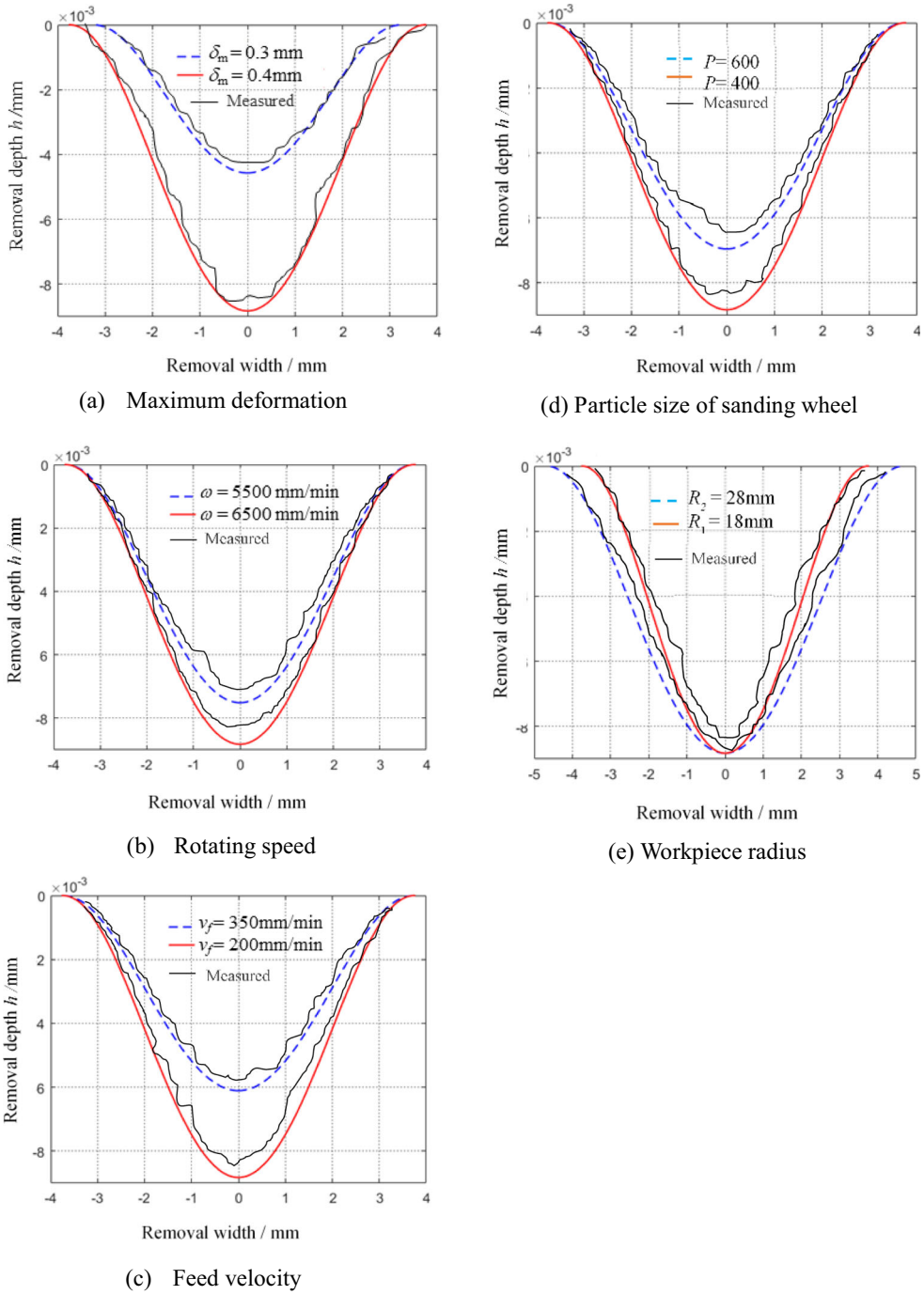

Fig. 8 Simulation and measured results of surface removal depth under different process parameters

3.1 Simulation test

The polishing process parameters used in the simulation test are listed in Table 2.

The simulation conditions are substituted into Eq. (6) to obtain the compression amount a_p as seen in Eq. (22).

$$a_p = \sqrt{{R_1}^2 - x^2} + \sqrt{{r_1}^2 - z^2} - R_1 - r_1 + \delta_m \tag{22}$$

According to the simulation conditions, the semi-major axis x_F and semi-minor axis z_G of the boundary in the elliptical contact zone can be obtained as seen in Eqs. (23) and (24), respectively.

$$x_F = \sqrt{\delta_m(2R_1 - \delta_m)} \tag{23}$$

$$z_G = \sqrt{\delta_m(2r_1 - \delta_m)} \tag{24}$$

The data in Table 1 and Eqs. (22), (23), and (24) are substituted into Eq. (21) to obtain the concrete expression of the removal depth.

The surface removal depths under different polishing process parameters can be acquired through the simulation (Fig. 8).

Figure 8 a indicates that with the increase of the maximum compression amount, both removal depth and width are increased obviously because with the increase of maximum compression amount, the contact area is enlarged, so is the area of the material removed. In Fig. 8 b–d, the width of the surface removal zone is not changed, but the removal depth is evidently reduced with the reduction of spindle speed and increase of feed velocity and abrasive particle size, and to figure out why, the spindle speed, feed velocity, and particle size almost have no influence on the turning radius of the sanding wheel; however, the lower the spindle speed or the higher the feed velocity, the smaller the quantity of the abrasive particles participating in cutting within unit time will be, and the larger the particle size, the smaller the volume of abrasive particle. Given this, the quantity of the material removed is reduced, so is the removal depth. Figure 8 e shows that under the same maximum compression amount, the larger the workpiece radius, the larger the boundary removed and the removal depth, because the larger the workpiece radius, the larger the contact area. Moreover, the compression amount at each point in the contact zone increases, both the contact boundary and removal depth will be increased.

3.2 Polishing test

The polishing test field is shown in Fig. 9. Marh XT20 is used to measure the removal depth, which passes through the contact point and is perpendicular to the direction of the polishing path. The radius of sanding wheel in NC programming is the rotation radius of sanding wheel minus the compression.

Fig. 9 Polishing test

During the polishing process, the flexible grinding head of the polishing machine tool adjusts the position and posture of the sanding wheel in real time according to the change of the blade profile, making the sanding wheel contact with the polishing surface; this ensures that the sanding wheel compression is constant throughout the polishing process.

Figure 10 displays the prediction and test results of the semi-major axis and semi-minor axis in the contact zone of the workpiece, indicating that as the maximum compression amount increases, the elliptical semi-major axis and semi-minor axis are also gradually enlarged, and that the variation trend of the measured data is identical with that of the theoretical data.

Ten groups of polishing process parameters in Table 2 are adopted to test the removal depth on 10 workpieces. The data measured via Marh XT20 is processed through the Matlab software, and the high-frequency signals are removed using Gaussian low-pass filter to acquire the surface profile shown as a black curve in Fig. 8. The contact zone on the workpiece surface is shown in Fig. 11.

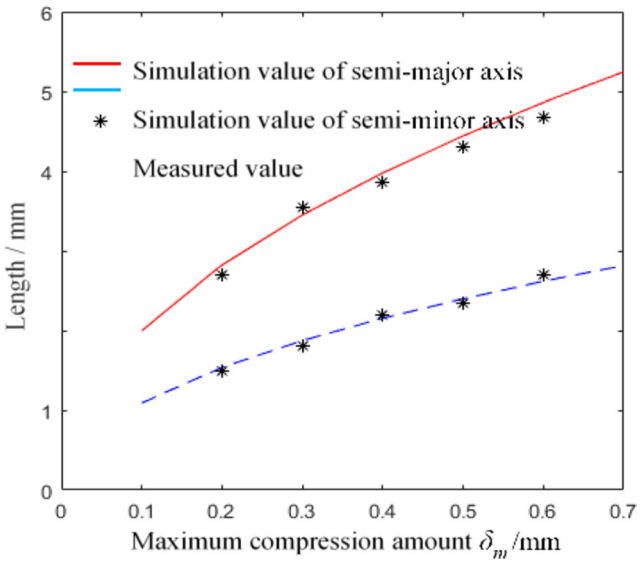

Fig. 10 Simulation results and test results of contact zone

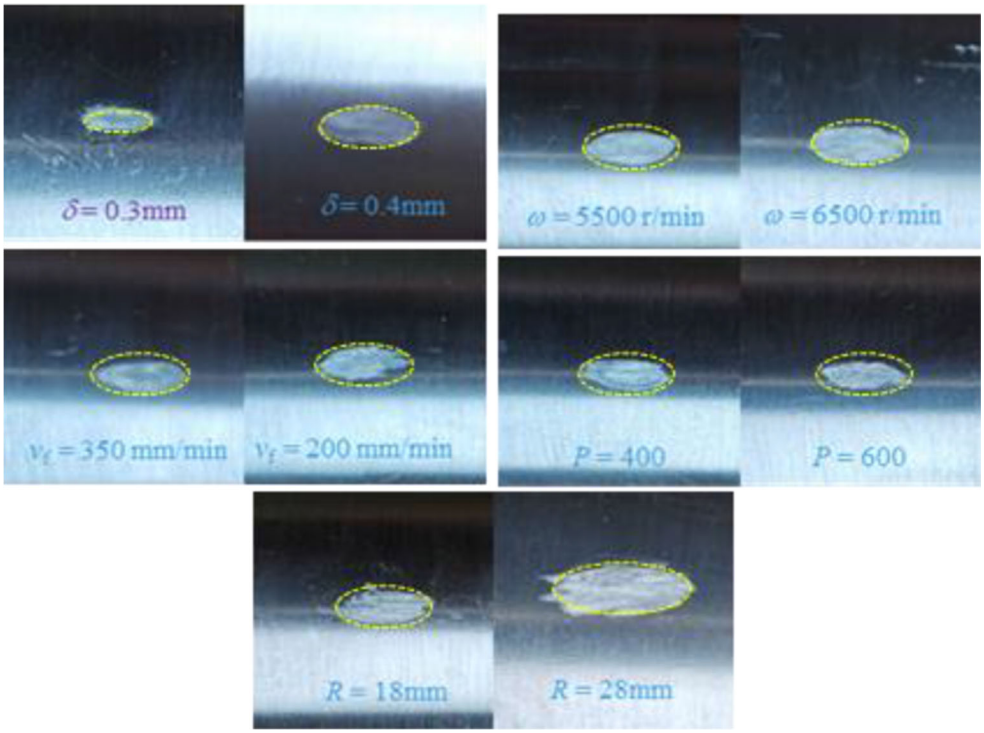

Fig. 11 Elliptical contact zone

As shown in Fig. 8, vibration will take place in the actual profile measurement process due to various interference factors such as the cylindrical surface errors of the sanding wheel and workpiece, abrasive wear, vibration of the sanding wheel, and dimensional error of the workpiece, and the measured result at the depth is smaller than the simulation result. Nevertheless, the profile of the post-filtering removal depth is consistent with the simulated profile. As shown in Fig. 11, the outline of contact zone on the workpiece surface is an ellipse, which is basically consistent with the theoretical outline.

Through the above comparison between the simulation test results and polishing test results, it is proved that the established boundary model and removal depth model in the surface contact zone are reliable and applicable to the prediction of geometric contact characteristics for the elastic grinding tool–polished complex surface.

4 Conclusions

1. According to the geometric contact model between the sanding wheel and polished surface, the semi-major axis and semi-minor axis of the boundary in the elliptical contact zone were calculated, and the mathematical model for the compression amount of the sanding wheel at any point and that for the material removal depth were established.
2. The influence mechanism of polishing process parameters on the boundary and removal depth in the contact zone was analyzed via a simulation test; the results show that the compression amount of the sanding wheel and the curvature radius of the workpiece surface both have remarkable effects on the boundary and removal depth in the contact zone, and the feed velocity, rotating speed, and particle size of the sanding wheel almost exert no influence on the removed profile, but they can influence the removal depth very significantly.
3. The polishing test results accord with the simulation results very well, which verifies that the reliability of the established geometric model for the flexible contact of the elastic grinding tool–polished complex surface.

Funding This work was jointly supported by the National Natural Science Foundation, China (No. 51675439).

References

1. Huai WB, Tang H, Shi YY (2017) Sensitivity of surface roughness to flexible polishing parameters of abrasive cloth wheel and their optimal intervals. J Mech Sci Technol 31(2):865–873
2. Liu D, Shi YY, Lin XJ, Xian C (2019) Study on improving surface residual stress of polished blade after polishing based on two-stage parameter method. Int J Adv Manuf Technol 100(5-8):1491–1503
3. Xiao GJ, Huang Y (2016) Equivalent self-adaptive belt grinding for the real-R edge of an aero-engine precision-forged blade. Int J Adv Manuf Technol 83(9-12):1697–1706

4. Huai WB, Tang H, Shi YY, Lin XJ (2017) Prediction of surface roughness ratio of polishing blade of abrasive cloth wheel and optimization of processing parameters. Int J Adv Manuf Techno 90(1-4):699–708
5. Kuo CC, Chen CM, Chang SX (2017) Polishing mechanism for ABS parts fabricated by additive manufacturing. Int J Adv Manuf Technol 91(5-8):1473–1479
6. Xiao GJ, Huang Y, Wang J (2018) Path planning method for longitudinal micromarks on blisk root-fillet with belt grinding. Int J Adv Manuf Technol 95(1-4):797–810
7. Liu GT, Li CH, Zhang YB, Yang M, Jia DZ, Zhang XP, Guo SM, Li RZ, Zhai H (2018) Process parameter optimization and experimental evaluation for nanofluid MQL in grinding Ti-6Al-4V based on grey relational analysis. Mater Manuf Process 33(9):950–963
8. Zhang JF, Shi YY, Lin XJ, Duan JH, Zhang HJ, Li ZS (2017) Optimization of blade belt polishing parameters based on grey relational analysis. Comput Integr Manuf Syst. 23(4):806–814 (in Chinese)
9. Zhao D, Guo H (2018) A trajectory planning method for polishing optical elements based on a non-uniform rational B-spline curve. Appl Sci 8(8):1355 14 pages
10. Gerhard C, Stappenbeck M (2018) Impact of the polishing suspension concentration on laser damage of classically manufactured and plasma post-processed zinc crown glass surfaces. Appl Sci 8(9): 1556 15 pages
11. Xiao GJ, He Y, Huang Y, Li W, Li Q Single particle removal model and experimental study on micro bionic zigzag surface of aeronautical blade using belt grinding. Acta Aeronautica et Astronautica Sinica http://kns.cnki.net/kcms/detail/11.1929.V.20190929.1657.008.html, (in Chinese)
12. Chen WC, Wu KL, Yan BH (2014) A study on the application of newly developed magneto-elastic abrasive to improving the surface roughness of the bore. Int J Adv Manuf Technol 73(9-12):1557–1566
13. Liu WN, Cai ZJ, Li YF Ren CZ (2017) Numerical simulation and experiments of abrasive flow polishing for nozzle micro-holes. China Mechanical Engineering 28(1):13-19,26 (in Chinese)
14. Qi JD, Zhang DH, Li S, Chen B (2016) A micro-model of the material removal depth for the polishing process. Int J Adv Manuf Technol 86(9-12):2759–2770
15. Huai WB, Shi YY, Tang H, Lin XJ (2019) An adaptive flexible polishing path programming method of the blisk blade using elastic grinding tools. J Mech Sci Technol 33(7):3487–3495
16. Wang YJ, Huang Y, Chen YX, Yang ZS (2016) Model of an abrasive belt grinding surface removal contour and its application. Int J Adv Manuf Technol 82(9-12):2113–2122
17. Xian C, Shi YY, Lin XJ, Liu D (2020) Experimental study on energy partition of polishing aero-engine blades with abrasive cloth wheel. Int J Adv Manuf Technol 106(5-6):1839–1853
18. Xian C, Shi YY, Lin XJ, Liu D (2020) Force modeling for polishing aero-engine blades with abrasive cloth wheels. Int J Adv Manuf Technol 106(11-12):5255–5267
19. Xian C, Shi YY, Lin XJ, Liu D (2020, 2020) Study on vibration characteristics of polishing rod for polishing aeroengine blade with abrasive cloth wheel. Math Probl Eng:5472502 14 pages